Development of a TFR-based method for the simultaneous detection of leakage and partial blockage in water supply pipelines

H. F. Duan, *M.ASCE*

Associate Professor, Department of Civil and Environmental Engineering, The Hong Kong Polytechnic University, Hung Hom, Kowloon, 999077 Hong Kong

Email: hf.duan@polyu.edu.hk

Abstract: Pipe leakage and partial blockage are the two common types of pipe defects in water supply systems. In practical systems, these defects, which may cause great waste of water and energy resources and can induce potential reduction of system operation capacity, are usually formed simultaneously. This paper develops an effective transient frequency response-based (TFR-based) method to characterize and detect simultaneously these two types of pipe defects. To this end, an analytical expression is firstly derived to characterize the simultaneous effect of leakage and partial blockage on TFR in water pipelines. The obtained results are then validated through laboratory experimental tests for the detection of multiple pipe defects. After validation, extensive numerical applications that cover typical ranges of test conditions are adopted to further investigate the applicability and accuracy of the developed TFR-based method. The application results demonstrate high accuracy and wide applicability of this TFR-based method to detect simultaneously potential leakage and partial blockage in water supply pipelines. The advantages and limitations of this TFR-based method are discussed in the final section for practical applications in urban water supply systems.

Keywords: Water pipeline; Transient frequency response (TFR); Leakage; Blockage; Detection

Introduction

In urban water supply systems (UWSS), pipelines commonly encounter many different problems that may affect the function and operation of UWSS, such as leakage, partial blockage and wall thinning, which are usually termed as pipe defects/faults in the literature (AWWA, 2012). These pipe defects could be formed easily in water supply pipeline due to various natural and artificial factors, including chemical corrosion, biofilm and physical deformation. The formation and existence of such pipe defects may result in serious problems, including (but not limited to) the reduction of flow capacity, increase of energy loss and deterioration of water quality (James and Shahzad, 2003). For example, in Hong Kong (HK), the annual cost for water and energy losses of its dual UWSS (i.e., fresh water and sea water conveyance systems) was estimated at over HK$ 1.5 billion (~US$ 200 million/year) (HKWSD, 2019). In the worldwide UWSS, the average water loss has been increased up to over 30% of the total supply amount (Gupta and Kulat, 2018). Therefore, it is urgent and important to develop effective technologies to diagnose these pipe defects in a timely manner, so as to minimize the resultant problems and wastage in the UWSS.

To solve above-mentioned critical issues in UWSS, different kinds of methods and tools have been developed to identify and assess water supply pipeline condition (Datta and Sarkar, 2016). The current commercially available technologies used for pipeline condition assessment mainly include two classes: (i) intrusive methods, such as CCTV cameras and Smart Balls (Stephens, 2008); and (ii) non-intrusive methods, e.g., moisture sensors, ground penetrating radar, and acoustic correlators (Puust et al., 2010). Indeed, the use of these methods and technologies has greatly reduced these problems in UWSS. However, current critical problem of water and energy losses (e.g., over 30% worldwide) has evidenced the inadequacy and inefficiency of these methods and tools in improving further the situations in UWSS (Datta and Sarkar, 2016).

Moreover, various previous applications in the literature have also demonstrated one or more following disadvantages for each of these current methods: (1) short-ranged and time-consuming to each test; (2) intrusive and expensive to practical system application; and (3) inapplicable/unreliable to identify simultaneously different types of pipe defects such as leakage and blockage (Stephens, 2008; Puust et al., 2010; Lee et al., 2013).

In recent years, a new and promising method that utilizes transient pressure waves, termed as transient-based method (TBM), to diagnose different problems UWSS has emerged. The tenet of this method is that an injected transient wave (with wave speed up to an order of 1000 m/s) propagating in pipelines is modified by, and thereby carries information about, the properties and states of these pipelines. This non-intrusive method allows potential pipe defects to be detected in a real-time manner and over a long range (Duan et al., 2010; Lee et al., 2013). With such advantages of this TBM, various researches and investigations have been performed for the pipeline condition assessment (e.g., leakage, partial blockage, wall thinning) through theoretical analysis, numerical simulation and modelling, and experimental applications (laboratory and field) (e.g., Liggett & Chen 1994; Brunone 1999; Vitkovsky et al., 2000; Mpesha et al. 2001; Wang et al. 2002; Adewumi et al., 2003; Lee et al. 2005, 2006; Duan et al. 2011, 2012a, 2014; Gong et al., 2013, 2014, 2016, 2018; Meniconi et al. 2015). In principle, the TBM in these previous studies can be classified into different types according to their utilization way of transient information: (1) time-domain method (TDM) (e.g., Liggett and Chen, 1994; Brunone, 1999; Kapelan et al., 2003; Massari et al., 2014); (2) frequency-domain method (FDM) (e.g., Lee et al., 2006, 2008; Sattar et al., 2008; Duan et al., 2011; Kim 2005, 2017; Duan 2016; Louati et al., 2017); and (3) time-frequency method (TFM) (e.g., Ghazali et al., 2012; Meniconi et al., 2013; Sun et al., 2016).

Till now, these studies in the literature have made substantial progress on the development and application of TBM for pipeline condition assessment (Datta and Sarkar, 2016). However, current TBM can largely be applied to simple situations of pipe defects with known specific type in the well-defined systems. In practical UWSS, the defects are usually formed from complicated processes; thereby, they may exist in multiple types in pipelines such as leakage, partial blockage and others. Under this practical situation, current TBM usually could not separate and detect them effectively (Stephen, 2008; Duan et al., 2017; Che et al., 2018). Accordingly, it has been widely observed in various laboratory/field tests and applications that this current method may lead to inaccurate or even invalid results for the detection of realistic anomalies (Stephen et al., 2012; Duan, 2017). This is mainly due to the incapability of current TBM for characterizing the potential information of different defects in pipelines (type, number, location and size). Therefore, it is important and urgent to develop an effective TBM for simultaneous detection of different types of pipe defects, so as to enhance the applicability and validity of this method (with high efficiency and low cost). This is the motivation and scope of current study.

This paper aims to develop a TBM utilizing transient frequency response (TFR) for the simultaneous detection of different pipe defects, which is termed as TFR-based method in this study. Two common types of pipe defects in UWSS – leakage and partial blockage – are adopted for the investigation. Through this study, it is expected to address the two following scientific and practical issues: (1) the possibility for separating the modification effects of these two different pipe defects in transient responses; (2) the development of an effective TFR-based method for detecting different pipe defects. For this purpose, an analytical expression of TFR for characterizing the frequency domain transient behaviors of leakage and partial blockage is firstly

95 derived in this study, and is then applied for inverse identification of these two types of pipe
96 defects. Note that only the discrete blockages, which are mainly due to partially closed inline
97 valve and/or rough joints along the pipeline (Meniconi et al., 2016), are considered for this
98 investigation. Thereafter, different laboratory and numerical experiments are conducted for the
99 validation and verification of the TFR-based method proposed in this study. Finally, the obtained
100 results are analyzed for discussion of for the application and implications of the extended TFR-
101 based method proposed in this paper.
102
103 **Models and Methods**
104 The transient model and transfer matrix method used for this study are presented in this section.
105
106 ***1D Transient Model and Numerical Scheme***
107 The one-dimensional (1D) water hammer model (also termed as transient model) is used for
108 analytical derivation and numerical simulation in this paper, which can be expressed as follows
109 (Wylie et al., 1993; Chaudhry, 2014):

110 $$\frac{gA}{a^2}\frac{\partial H}{\partial t}+\frac{\partial Q}{\partial x}=0 \tag{1}$$

111 $$\frac{\partial Q}{\partial t}+gA\frac{\partial H}{\partial x}+\frac{\pi D}{\rho}\tau_w=0 \tag{2}$$

112 in which: Q, H = discharge and pressure head; x, t = spatial and time coordinates; D, A = pipe
113 diameter and cross-sectional area; g = gravitational acceleration; a = wave speed; ρ = density;
114 and τ_w = wall shear stress, which can be expressed as (Zielke, 1968; Vardy and Brown, 2003):

115 $$\tau_w=\tau_{ws}+\tau_{wu} \tag{3}$$

with τ_{ws} and τ_{wu} being the quasi-steady and unsteady components of τ_w, respectively. For turbulent flows, the quasi-steady wall shear stress is commonly simulated by the Darcy-Weisbach equation as (Wylie et al., 1993; Chaudhry, 2014),

$$\tau_{ws} = \frac{\rho f}{8A^2} Q|Q| = sign(Q)\frac{\rho f Q^2}{8A^2} \tag{4}$$

with f being the Darcy friction factor at initial flow state and *sign*() for the sign function. In this study, the pipelines for all tests are assumed to be smooth and thus the value of f can be determined by the Kármán–Prandtl resistance equation. For modelling the unsteady wall shear stress, the weighting function based (WFB) model is adopted by (Vardy and Brown, 2003),

$$\tau_{wu} = \frac{4\rho\nu}{DA}\int_0^t W(t-t')\frac{\partial Q(t')}{\partial t'}dt' \tag{5}$$

where $W(t) = \phi e^{-\lambda t}/\sqrt{\pi t}$ is weighting function with ϕ, λ being convolution coefficients for various flow regimes, with $\phi = D/4\sqrt{\nu}$, $\lambda = (0.54\nu k_{\mathrm{Re}})/D^2$ and $k_{\mathrm{Re}} = \mathrm{Re}^{\log(14.3/\mathrm{Re}^{0.05})}$; $\mathrm{Re} = QD/Av$ is Reynolds number; v is kinematic viscosity; and t' is a dummy time variable.

The MOC scheme is used for the 1D numerical simulation in the time domain (Chaudhry, 2014), where the nonlinear turbulent friction term in Eq. (4) is treated discretely by a 2nd-order approximation and the unsteady friction term in Eq. (5) is dealt with by the full convolution of historical time effect (Vardy and Brown, 2003; Wylie et al., 1993). The MOC-based numerical simulation method has been widely studied and fully validated for its accuracy and validity in the literature (Chaudhry, 2014) and is used for the evaluation and validation of the proposed TFR-based method later in this study.

Transfer Matrix Method

For the convenience of conducting analytical analysis, the following transient perturbations are defined ("*" represents perturbation variable and "$_0$" represents steady state quantity):

$$H = H_0 + h^*;\ Q = Q_0 + q^*$$

Substituting these variables into Eq. (1) – Eq. (3) and neglecting the nonlinear terms (i.e., order ≥ 2), we obtain,

$$\frac{gA}{a^2}\frac{\partial h^*}{\partial t} + \frac{\partial q^*}{\partial x} = 0 \tag{6}$$

$$\frac{1}{gA}\frac{\partial q^*}{\partial t} + \frac{\partial h^*}{\partial x} + \frac{4}{\rho g D}\tau^* = 0 \tag{7}$$

with τ^* being converted shear stress term. By applying the transfer matrix method to these two equations (Lee et al., 2006; Duan et al., 2011; Chaudhry, 2014), we obtain the equivalent frequency domain results of transient response in a pipeline section,

$$\begin{Bmatrix} q \\ h \end{Bmatrix}^{n+1} = \begin{bmatrix} \cos(\mu x_m) & i\frac{1}{Y}\sin(\mu x_m) \\ iY\sin(\mu x_m) & \cos(\mu x_m) \end{bmatrix} \begin{Bmatrix} q \\ h \end{Bmatrix}^{n} \tag{8}$$

where q, h = discharge and pressure head perturbations in frequency domain; n, n+1 = index numbers of upstream and downstream end of pipe section; x_m = length of pipeline; i = imaginary unit; Y, μ = impedance and propagation factor of pipeline, which can be given by,

$$\mu = \frac{\omega}{a}\sqrt{1 - iR_f};\ \ Y = -\frac{a}{gA}\sqrt{1 - iR_f} \tag{9}$$

in which ω = frequency; R_f = friction resistance factor, and,

$$R_f = \frac{fQ_0}{\omega DA} + \frac{16 i \nu \phi}{D^2\sqrt{\lambda + i\omega}} \tag{10}$$

155 **TFR-Based Method Development**

156 In this study, the simple reservoir-pipeline-valve (RPV) system with two types of defects
157 (leakage and partial blockage) is adopted for the demonstration of method principle development
158 and application procedure. Note that the derived results are extendable to relatively complex
159 systems with multiple pipelines based on the former study of Duan (2017), as long as a clear
160 incident wave form with relatively large bandwidth can be generated and an appropriate signal
161 processing method can be applied for the wave analysis (Lee et al., 2013 and 2015). To this end,
162 the RPV systems with and without pipe defects sketched in Fig. 1 are used for the investigation
163 in the following study. For clarity, only the key results are presented in this section, while the
164 details about the analytical derivations are provided in the appendix section at the end of this
165 paper.

166 [Fig. 1 will be about here]

167

168 ***TFR Results for Intact and Defective Systems***

169 The TFR for intact RPV system has been widely developed and used in the literature (e.g., Lee et
170 al., 2006; Duan et al., 2012a; Chaudhry, 2014; Duan and Lee, 2016). Particularly, the resonance
171 condition for the system in Fig. 1(a) is known as:

172 $$\cos(\mu L) = 0 \tag{11}$$

173 For defective pipeline systems, two cases in Fig. 1(b) and Fig. 1(c), denoted as Case *A*
174 and Case *B*, are considered to examine the impact of relative positions of different defects on the
175 TFR results. Prior to deriving the TFR results for these two cases, it is necessary to define the
176 transfer matrix for each of the defects (leakage and partial blockage) (Lee et al., 2006 and 2008),
177 which can be summarized as follows:

178 $$\begin{bmatrix} 1 & K \\ 0 & 1 \end{bmatrix}; \quad \begin{bmatrix} 1 & 0 \\ I & 1 \end{bmatrix} \tag{12}$$

179 where K is the impedance factor of leakage orifice and $K = -Q_{l0}/2\Delta H_{l0}$ with Q_{L0} and ΔH_{L0} are
180 steady state discharge and head difference at the leakage orifice; I is the impedance factor of
181 discrete blockage, and $I = -2\Delta H_{b0}/Q_{b0}$ with ΔH_{b0} and Q_{b0} are steady state minor head loss and
182 discharge at the blockage location. Note that these two impedance factors (K and I) are obtained
183 through a linearization operation of the orifice equation as in Lee et al. (2006, 2013).

184

185 *Results for Case A in Fig. 1(b)*

186 By applying the analytical analysis as conducted in former studies (Duan et al., 2014; Chaudhry,
187 2014), the overall transfer matrix for the system in Fig. 1(b) is given by,

188 $$\begin{Bmatrix} q \\ h \end{Bmatrix}^{Dn} = \begin{bmatrix} U_{11} & U_{12} \\ U_{21} & U_{22} \end{bmatrix} \begin{Bmatrix} q \\ h \end{Bmatrix}^{Up} \tag{13}$$

189 with the matrix elements ($U_{11} \sim U_{22}$) given in the appendix. The application of the boundary
190 conditions of the system in Fig. 1(b) (i.e., $h^{Up} = q^{Dn} = 0$), gives (subscript "$_A$" denotes results for
191 case A, and superscript "^{Dn}" represents the results for downstream end),

192 $$h_A^{Dn} = -\frac{U_{21}}{U_{11}} \tag{14}$$

193 Considering in the realistic water supply systems that, $K \ll Y$, $I \ll Y$ and $KI \ll 1$, we
194 obtain the TFR for this defective pipeline system as (by taking pressure head for illustration),

195 $$\hat{h}_A = \frac{1}{\left|h_A^{Dn}\right|} = \left| K \sin(\mu x_1)\cos(\mu y_2 + \mu d) + \frac{I}{Y^2}\cos(\mu x_1 + \mu d)\sin(\mu y_2) \right| \tag{15}$$

196 where $\hat{h}$ is inverted transient pressure head in the frequency domain. A further discussion about
197 the validity and accuracy of this imposed assumption of $KI \ll 1$ is performed later in this paper.

198

199 *Results for Case B in Fig. 1(c)*

200 Similar analysis can be applied in the other system condition in Fig. 1(c), which leads to the final

201 TFR result as (subscript "$_B$" denotes results of case *B*),

202 $$\hat{h}_B = \frac{1}{\left|h_B^{Dn}\right|} = \left| K\cos(\mu x_2)\sin(\mu y_1 + \mu d) + \frac{I}{Y^2}\cos(\mu y_1)\sin(\mu x_2 + \mu d) \right| \tag{16}$$

203 Therefore, Eq. (15) and Eq. (16) are referred to as the TFR patterns for the RPV systems

204 with two different types of pipe defects (leakage and partial blockage) in the system.

205

206 ***TFR Results Analysis and Application Procedure***

207 The forms of the obtained TFR patterns in Eq. (15) and Eq. (16) are similar, but the parameters

208 and mathematical details in current forms are different from each other. To fairly compare and

209 examine the influence of the relative positions of two defects, it is necessary to convert the forms

210 into unified parameters. For this purpose, the two patterns are rewritten as follows:

211 $$\hat{h}_A = \left| KF_{A1} + \frac{I}{Y^2}F_{A2} \right|;\ \text{and}\ \hat{h}_B = \left| KF_{B1} + \frac{I}{Y^2}F_{B2} \right| \tag{17}$$

212 where F_{A1}, F_{A2}, F_{B1} and F_{B2} are intermediate parameters for further analysis. That is,

213 $$\begin{matrix} F_{A1} = \sin(\mu x_1)\cos(\mu y_2 + \mu d) \\ F_{A2} = \cos(\mu x_1 + \mu d)\sin(\mu y_2) \end{matrix}; \quad \begin{matrix} F_{B1} = \cos(\mu x_2)\sin(\mu y_1 + \mu d) \\ F_{B2} = \cos(\mu y_1)\sin(\mu x_2 + \mu d) \end{matrix}$$

214 From the system information shown in Fig. 1, it is easy to obtain the following relations: $y_2 + d =$

215 x_2 and $x_1 + d = y_1$ for Case A; $y_1 + d = x_1$ and $x_2 + d = y_2$ for Case B. Further mathematical

216 operation and rearrangement gives, $F_{A1} = F_{B1}$ and $F_{A2} = F_{B2}$. That is, $\hat{h}_A = \hat{h}_B$.

217 As a result, the above two TFR patterns provide a unified form as follows,

$$\hat{h} = \frac{1}{\left|h^{Dn}\right|} = \left| K \frac{(-1)^m + \sin(\mu x_1 - \mu x_2)}{2} + \frac{I}{Y^2} \frac{(-1)^m + \sin(\mu y_2 - \mu y_1)}{2} \right| \tag{18}$$

where m is the number of transient frequency peaks (i.e., peaks under resonance condition). Consequently, the overall TFR pattern induced by multiple types of pipe defects in the PRV system is composed of a linear combination of their respective TFR patterns. This finding of Eq. (18) confirms the possibility and also provides the way to separate the influences of different defects for pipeline condition assessment, which is actually the principle of multi-defects detection method in this study.

The obtained TFR pattern in Eq. (18) indicates the dependent relationship of transient frequency peaks on the leakage and partial blockage information (size, location) as well as intact system information (wave impedance). Therefore, the potential leakage and partial blockage information (type, number, size, and location) can be inversely determined by measuring the transient frequency response and knowing the original intact pipeline system parameters. For this inverse analysis of pipe defects, the genetic algorithm (GA) based optimization technique is applied in this study, with the aim to minimize the difference between measured and calculated results of transient frequency peaks, which can be formulated as follows (Duan and Lee, 2016):

$$Min \quad \sum_m \left| \hat{h}_p - \hat{h}_e \right| \tag{19}$$

where $\hat{h}_p$ and $\hat{h}_e$ are inverted transient peak amplitudes from the results of the analytical Eq. (18) and the experimental measurement respectively. For GA-based inverse calibration, the decision variables and searching ranges are specified as,

(1) Locations of leakage and blockage: $0 < x_1, x_2 < L$; $0 < y_1, y_2 < L$;

(2) Sizes of leakage and blockage: $0 < Q_{l0}/Q_0 < 50\%$; $0 < \Delta H_{b0}/H_0 < 50\%$;

239 (3) Numbers of leakage and blockage: $0 \le M_{LEAK} \le 2; 0 \le M_{BLOCK} \le 2$.

240 For each test system, other information such as intact system configuration and initial steady
241 flow conditions are known in advance to the detection method above.

242 The developed GA-based optimization method and procedure in former studies in this
243 field (e.g., Duan et al., 2012a; Duan and Lee, 2016) is adopted for this investigation. Prior to the
244 extensive applications later in this paper, the GA-based optimization framework has been
245 carefully tested for fitting in the inherent parameters and coefficients of the algorithm (Vitkovsky
246 et al., 2000; Kapelan et al., 2003), in order to ensure its applicability and accuracy in this study.

247

248 **Applications and Results**

249 To examine the capability of the developed TFR-based method in Eq. (18) for the multi-type
250 defects detection, laboratory experimental tests are firstly applied to verify and validate the
251 developed TFR-based method in this study. After validation, extensive numerical experiments
252 are then applied to further analyze the validity and accuracy of this developed method under
253 various systems and flow conditions, which may cover a practical range of system settings and
254 operations (e.g., pipe scales and flow conditions).

255 In the applications, time-domain transient signals (e.g., pressure head series) are obtained
256 from measurement for the experimental application and from numerical simulations by the
257 MOC-based 1D transient model of Eq. (1) and Eq. (2) for numerical applications. For testing,
258 transients are generated at the downstream of the pipeline as shown in Fig. 1, and the pressure
259 head traces are collected at the same location for the analysis. The obtained time-domain results
260 are then transformed into the frequency domain equivalences using the method presented in the
261 former studies (e.g., Lee et al., 2013) and the frequency peaks are then extracted to fit the derived

262 Eq. (18), thereby to obtain the type, number, size and location of potential defects in the system.

263

264 ***Preliminary Experimental Verification***

265 The laboratory experimental system and measurement dataset in the previous study of Sun et al.
266 (2016) are used for preliminary experimental verification in this study. The test pipeline system
267 and associated facilities are sketched in Fig. 2, consisting of an upstream pressure vessel, a
268 pipeline divided into different sections for testing, a downstream discharge tank, and a water
269 recycling pump. Transients are generated by the fast closure of an inline valve installed at the
270 downstream from initially full open state within 0.1 s. The transient pressure head signals are
271 measured and collected at two ends of the test pipeline (upstream and downstream). The relevant
272 data information of the test system is given in Fig. 2. For this study, two different cases including
273 one leakage and one partial blockage (mimicked by a pipe-wall orifice and an inline valve,
274 respectively) are placed in the system, with the real values of these two defects shown in Table 1.
275 For each case, multiple tests have been repeated for reducing the possible operation errors and
276 system noises. The measured pressure signals selected from the multiple tests for these two cases
277 are shown in Fig. 3.

278 [Table 1 will be about here]

279 [Fig. 2 will be about here]

280 [Fig. 3 will be about here]

281 Based on the developed TFR-based method and the proposed application procedure
282 above, the detection results of these two defects can be obtained for analysis. For evaluation, the
283 inaccuracy of the developed method (i.e., application error ε) is defined by the relative difference
284 between the real and predicted values of two defects, as follows:

$$\varepsilon(\%) = \frac{\text{predicted value - real value}}{\text{real value}} \times 100 . \quad (20)$$

Based on Eq. (20), the prediction errors for the information of these two defects (location and size) are calculated and shown in Table 1. Meanwhile, the obtained TFR patterns for these two cases are shown in Figs. 4(a) and 4(b) respectively. Overall, the proposed method could provide acceptable results for the multiple-defects detection in the tested pipeline system under different flow and defective conditions. Specifically, the developed TFR-based method can identify exactly and simultaneously the number and types of the two detects in the pipeline (i.e., one leakage and one partial blockage). Furthermore, the maximum relative errors of the predicted location and size of these defects are around 4.5% and 10.5%. This result indicates a relatively high detection accuracy of the developed TFR-based method in this study.

[Fig. 4 will be about here]

From the results in Table 1, it is also noted that the prediction of defect location by this method is more accurate than that of defect size. This finding is actually consistent with many previous studies regarding different detection methods for single type of defects (e.g., Duan et al., 2011, 2012a; Meniconi et al., 2013; Gong et al., 2016). This is mainly due to the potential inaccuracy of current 1D transient model and theory for representing energy dissipation/damping in practical pipe systems (e.g., minor loss, unsteady friction and turbulence). The influences of different system and flow conditions to the applicability of this developed TFR-based method are examined in details through extensive numerical applications in the following section.

Numerical Applications and Results Analysis

The RPV system shown in Fig. 1 is adopted for the numerical investigation. The available

307 pressure head at the upstream reservoir in Fig. 1 is set as H_0 = 100 m. For the analysis in this
308 paper, in total 8 numerical tests listed in Table 2 (denoted as tests N1 to N8) are selected from
309 various numerical applications for conducting this study, in following conditions:

310 (1) Pipeline scale L/D: $10^2 \sim 10^4$;

311 (2) Initial flow condition Re_0: $10^4 \sim 10^6$;

312 (3) Leakage percentage $Q_{l0}/Q_0 = |2KH_0/Q_0|$: 5% ~ 30%;

313 (4) Blockage loss percentage $\Delta H_{b0}/H_0 = |IQ_0/2H_0|$: 5% ~ 20%.

314 It is also noted that the tests N1 and N2 in Table 2 are respectively designed for the special
315 situations with only one of two types of defects, so as to conduct a comparative analysis with
316 former studies (e.g., Lee et al., 2006; Duan et al., 2011; Chaudhry, 2014).

317 [Table 2 will be about here]

318 Based on the proposed TFR-based method, the information of defects for each test
319 (defect type, size, and location) in Table 2 can be obtained for analysis. For illustration, case N3
320 in Table 2 is adopted herein for example. Firstly, the transient pressure head at the downstream
321 valve is collected from the 1D numerical modelling, which is then transformed into the
322 frequency domain so as to obtain the TFR result (Lee et al., 2013). Accordingly, the first 15
323 frequency peaks of the obtained TFR results are extracted and converted (as "real values"),
324 which are thereafter fitted by the analytical TFR result of Eq. (18) (as "predicted values") based
325 on the proposed GA-based optimization framework. The results of extracted and fitted TFR
326 patterns are shown in Fig. 5 for comparison.

327 [Fig. 5 will be about here]

328 As a result, the predicted values of the information of potential defects in pipeline for
329 case N3 can be obtained as follows:

330 *Leakage*: $x_1/L = 0.208$ m (3.50%); $K = -7.610\times10^{-7}$ m^2/s (3.23%)

331 *Blockage*: $y_1/L = 0.715$ m (2.14%); $I = -1.216\times10^{5}$ m^2/s (4.49%)

332 in which the numbers in brackets refer to the relative errors of the prediction results. Both
333 the TFR patterns in Fig. 5 and the prediction results above indicate the high accuracy and
334 applicability of the developed TFR-based method in this study for the detection of multiple
335 defects in pipelines. It is also observed from Fig. 5 that the fitting accuracy of the TFR pattern
336 decreases gradually with peak number (e.g., after 10th peaks). This discrepancy can be mainly
337 attributed to: (1) the error of the 1D numerical model for representing the high frequency wave
338 modes in pipelines with different defects under the given/fixed simulation scheme. That is, the
339 numerical discretization error becomes more significant for higher frequency wave modes; (2)
340 the relatively high sensitivity of TBM to the low frequency mode of transient responses (Duan,
341 2015, 2016; 2017), such that the fitting accuracy becomes higher for the lower frequency peaks
342 in the TFR patterns; and (3) the error/inaccuracy of the GA-based optimization algorithm, which
343 can usually provide only a quasi-optimal solution for the complex inverse problem analysis. In
344 other words, the detection accuracy of this TFR-based method can be further improved by
345 employing more advanced inverse fitting techniques, which is however out of the scope of the
346 current study.

347 [Fig. 6 will be about here]

348 By applying the above similar analysis process to all other cases in Table 2, the
349 prediction errors for the location and size of two different defects are evaluated and shown in Fig.
350 6(a) and Fig. 6(b) respectively. By inspection, the results of all test cases in Fig. 6 show that the
351 maximum relative errors are about 10% and 20% for predicting the location and size information
352 of the potential defects respectively. These results confirm again the high accuracy and

353 applicability of the developed TFR-based method in this study. By comparison, the results also
354 reveal that the accuracy of this method becomes better (for both location and size detection) for
355 the single type of defects (cases N1 and N2 in Table 2) than other cases with two types of defects
356 (cases N3 ~ N8 in Table 2). In the data analysis among all these tests, the errors can be attributed
357 to two main factors as follows: (1) analytical derivation errors induced by the linearization and
358 approximation of pressure-discharge relationship for the two types of defects (Duan et al., 2018);
359 (2) optimization-based data fitting errors for the analytical Eq. (18) (Duan and Lee, 2016); and (3)
360 uncertainty of the data treatment and analysis such as truncation and discretization errors (Duan,
361 2015, 2016). As a result, for the cases of multiple types of pipe defects, the errors caused
362 simultaneously by these two factors become more significant, and thereby the detection accuracy
363 can be reduced compared with the one single defect cases.
364
365 ***Further Results Discussion***
366 Despite the high accuracy of the detection results, the errors of both defect location and size
367 detection in Fig. 6 vary greatly in different cases. Therefore, it is necessary to examine the
368 influences of the system and flow conditons from all the tests about the detection accuracy of the
369 developed TFR-based method. Based on the preliminary analysis in this study, the parameters
370 affecting such accruacy can be divided into two groups: (1) the test system and flow condition;
371 and (2) the TFR method accuracy. For the first group, the former study of Duan et al. (2012b)
372 has demonstranted that the effect of system and flow conditions can be lumped into a
373 dimensionless parameter, defined as: $f\mathrm{Re}_0 T_w/T_d$, where T_w and T_d are time scales for wave
374 propagation and radial diffusion during the transient process. For the second group, based on the
375 derivation process of the TFR method in this study, the key term/parameter relating to the

376 linearization and simplification, which has been neglected in final result of Eq. (18), is the
377 product of leakage and blockage impedance factors: *KI*.

378 [Fig. 7 will be about here]

379 For all the multiple-defect tests in Table 2 (i.e., N3~N8), the variations of the detection
380 errors with these two parameters are calculated and shown in Fig. 7. On one hand, as indicated in
381 Fig. 7(a), the detection error (or accuracy) is significantly increasing (or decreasing) with the
382 dimensionless parameter $f\mathrm{Re}_0 T_w/T_d$. This also means the developed TFR method becomes more
383 accurate used in relatively smaller scale pipelines (e.g., smaller L/D) under lower initial flowrate
384 conditions (e.g., smaller Re_0). For better explanation, according to Duan et al., (2012b), for the
385 situation with smaller $f\mathrm{Re}_0 T_w/T_d$, the contribution of the nonlinear quasi-steady friction in Eq. (4)
386 relative to the linear convelution based unsteady friction in Eq. (5) becomes smaller, and thereby,
387 the errors due to the linearzation in the final analytical result of Eq. (18) become relatively
388 smaller.

389 On the other hand, the results of Fig. 7(b) demonstrate an increasing trend of the errors
390 with the parameter *KI*. This is not a surprise because all the nonlinear terms related to this
391 parameter KI during the analytical derivation process have been ignored under the assumption
392 that $K << 1$, $I << 1$ and thus $KI << 1$. Therefore, when this parameter *KI* becomes larger and
393 significant (e.g., close to 1), this imposed assumption will become problematic (or not accurate
394 enough) for representing the actual TFR pattern by the two types of defects. For example, for the
395 test case N8 in Table 2, the value *KI* attains to around 0.3, which leads to an overall errors of
396 about 15% and 20% for predicting the defect location and size respectively.

397 The results and analysis from both laboratory experiments and numerical applications in
398 this study demonstrate the good accuracy and applicability of the developed TFR-based method

399 for the simultaneous detection of multiple-type of defects in pipelines. However, these results
400 and discusson also indicate the potential limitations of this proposed TFR-based method for
401 practical applications. That is, this developed method is mainly applicable to: (1) simple piplilne
402 system (with single pipeline configuration); (2) relatively small to moderate severity and extent
403 of defects (e.g., with $K << 1$ and $I << 1$); and (3) relatively low to moderate turbulent flows (e.g.,
404 $\mathrm{Re}_0 < 10^6$). Consequently, for practical applications such as field tests, it is necessary to examine
405 in advance the system and flow conditions under investigation based on the two proposed
406 parameters (i.e., $f\mathrm{Re}_0 T_w/T_d$ and KI), so as to better understand and use of the developed TFR-
407 based method in this study.
408
409 **Conclusions**
410 In practical water supply systems, different types of pipe defects such as leakage and partial
411 blockage are usually formed simultaneously in the pipeline under various complex conditions.
412 This paper develops an effective method for the simultaneous detection of two common types of
413 defects (i.e., leakage and partial blockage) in pipelines. To this end, theoretical analysis is firstly
414 performed based on 1D transient model to obtain an analytical expression that characterizes the
415 influences of these two types of defects to transient frequency response (TFR). This developed
416 TFR method has been validated by different laboratory experiments for its applicability and
417 accuracy. After validation, extensive numerical applications are used to further examine the
418 validity and accuracy of this TFR-based method developed in this study.
419 Both the experimental and numerical application results demonstrate the high accuracy of
420 the developed TFR-based method for and detecting the two types of defects in pipelines under
421 different systems and flow conditions. Moreover, two lumped parameters ($f\mathrm{Re}_0 T_w/T_d$ and KI) are

422 proposed and used to characterize the applicability of this developed method. Specifically, the
423 maximum error of defect location detection for all the test cases of interest in this study is within
424 10%, and that of defect size detection can also be confined to less than 10% as long as the
425 lumped impedance parameter KI is much less than 1 (e.g., $KI < 0.25$ based on extensive
426 numerical tests in this study). Furthermore, the results and analysis also indicate that the
427 developed TFR-based method become more accurate for relatively smaller scale pipelines under
428 lower initial flow conditions.

429 Based on the results and findings of this study, it is also suggested that more experimental
430 validations (both laboratory and field tests) are required in future work to further examine and
431 confirm the validity and accuracy of the proposed TFR-based method in this paper.

432

433 **Data Availability Statement**

434 Some or all data, models, or code generated or used during the study are available from the
435 corresponding author by request (including analytical derivation and numerical test data).

436

437 **Acknowledgements**

438 This research work was supported by the Hong Kong Research Grants Council (RGC) under
439 projects 25200616, 15201017, and T21-602/15R.

440

441 **Appendix – Analytical Derivation of TFR Results**

442 The key steps of deriving the final TFR result in Eq. (18) are elaborated in this section. Based on
443 the principle of transfer matrix analysis in the literature (Lee et al., 2013; Chaudhry, 2014), the
444 results of the two cases in Fig. 1(b) and Fig. 1(c) are given as follows.

(1) For the case A in Fig. 1(b), the overall transfer matrix is,

$$\begin{Bmatrix} q \\ h \end{Bmatrix}^{Dn} = \begin{bmatrix} \cos(\mu y_2) & i\frac{1}{Y}\sin(\mu y_2) \\ iY\sin(\mu y_2) & \cos(\mu y_2) \end{bmatrix} \begin{bmatrix} 1 & 0 \\ I & 1 \end{bmatrix} \begin{bmatrix} \cos(\mu d) & i\frac{1}{Y}\sin(\mu d) \\ iY\sin(\mu d) & \cos(\mu d) \end{bmatrix} \begin{bmatrix} 1 & K \\ 0 & 1 \end{bmatrix} \begin{bmatrix} \cos(\mu x_1) & i\frac{1}{Y}\sin(\mu x_1) \\ iY\sin(\mu x_1) & \cos(\mu x_1) \end{bmatrix} \begin{Bmatrix} q \\ h \end{Bmatrix}^{Up} \tag{21}$$

with $d = y_1 - x_1 = 1 - y_2 - x_1$ is the distance between the two defects in this case shown in Fig. 1(b), and other symbols can be referred to their definitions in this paper. After mathematical manipulation, the result becomes,

$$\begin{Bmatrix} q \\ h \end{Bmatrix}^{Dn} = \begin{bmatrix} U_{11} & U_{12} \\ U_{21} & U_{22} \end{bmatrix} \begin{Bmatrix} q \\ h \end{Bmatrix}^{Up} \tag{22}$$

where the matrix elements are expressed as follows:

$$U_{11} = \left[\cos(\mu y_2 + \mu d) + i\frac{I}{Y}\sin(\mu y_2)\cos(\mu d)\right]\left[\cos(\mu x_1) + iKY\sin(\mu x_1)\right] + iY\sin(\mu x_1)\left[i\frac{1}{Y}\sin(\mu y_2 + \mu d) - \frac{I}{Y^2}\sin(\mu y_2)\sin(\mu d)\right];$$

$$U_{21} = \left[iY\sin(\mu y_2 + \mu d) + I\cos(\mu y_2)\cos(\mu d)\right]\left[\cos(\mu x_1) + iKY\sin(\mu x_1)\right] + iY\sin(\mu x_1)\left[\cos(\mu y_2 + \mu d) + i\frac{I}{Y}\cos(\mu y_2)\sin(\mu d)\right];$$

$$U_{12} = \left[\cos(\mu y_2 + \mu d) + i\frac{I}{Y}\sin(\mu y_2)\cos(\mu d)\right]\left[i\frac{1}{Y}\sin(\mu x_1) + K\cos(\mu x_1)\right] + \cos(\mu x_1)\left[i\frac{1}{Y}\sin(\mu y_2 + \mu d) - \frac{I}{Y^2}\sin(\mu y_2)\sin(\mu d)\right];$$

$$U_{22} = \left[iY\sin(\mu y_2 + \mu d) + I\cos(\mu y_2)\cos(\mu d)\right]\left[i\frac{1}{Y}\sin(\mu x_1) + K\cos(\mu x_1)\right] + \cos(\mu x_1)\left[\cos(\mu y_2 + \mu d) + i\frac{I}{Y}\cos(\mu y_2)\sin(\mu d)\right].$$

456 (2) For the case B in Fig. 1(c), the overall transfer matrix is,

$$\begin{Bmatrix} q \\ h \end{Bmatrix}^{Dn} = \begin{bmatrix} \cos(\mu x_2) & i\frac{1}{Y}\sin(\mu x_2) \\ iY\sin(\mu x_2) & \cos(\mu x_2) \end{bmatrix} \begin{bmatrix} 1 & K \\ 0 & 1 \end{bmatrix} \begin{bmatrix} \cos(\mu d) & i\frac{1}{Y}\sin(\mu d) \\ iY\sin(\mu d) & \cos(\mu d) \end{bmatrix}$$

457 $$\begin{bmatrix} 1 & 0 \\ I & 1 \end{bmatrix} \begin{bmatrix} \cos(\mu y_1) & i\frac{1}{Y}\sin(\mu y_1) \\ iY\sin(\mu y_1) & \cos(\mu y_1) \end{bmatrix} \begin{Bmatrix} q \\ h \end{Bmatrix}^{Up} \quad (23)$$

458 with $d = x_1 - y_1 = 1 - x_2 - y_1$ for this case. As a result,

$$\begin{Bmatrix} q \\ h \end{Bmatrix}^{Dn} = \begin{bmatrix} U_{11}^* & U_{12}^* \\ U_{21}^* & U_{22}^* \end{bmatrix} \begin{Bmatrix} q \\ h \end{Bmatrix}^{Up} \quad (24)$$

459

460 where the matrix elements are expressed as follows,

$$U_{11}^* = \left[\cos(\mu x_2 + \mu d) + iKY\cos(\mu x_2)\sin(\mu d)\right]\cos(\mu y_1)$$

461 $$+\left[i\frac{1}{Y}\sin(\mu x_2 + \mu d) + K\cos(\mu x_2)\cos(\mu d)\right]\left[I\cos(\mu y_1) + iY\sin(\mu y_1)\right];$$

$$U_{21}^* = \left[iY\sin(\mu x_2 + \mu d) - KY^2\sin(\mu x_2)\sin(\mu d)\right]\cos(\mu y_1)$$

462 $$+\left[\cos(\mu x_2 + \mu d) + iKY\sin(\mu x_2)\cos(\mu d)\right]\left[I\cos(\mu y_1) + iY\sin(\mu y_1)\right];$$

$$U_{12}^* = \left[\cos(\mu x_2 + \mu d) + iKY\cos(\mu x_2)\sin(\mu d)\right]i\frac{1}{Y}\sin(\mu y_1)$$

463 $$+\left[i\frac{1}{Y}\cos(\mu x_2 + \mu d) + K\cos(\mu x_2)\cos(\mu d)\right]\left[\cos(\mu y_1) + i\frac{I}{Y}\sin(\mu y_1)\right];$$

$$U_{22}^* = \left[iY\sin(\mu x_2 + \mu d) - KY^2\sin(\mu x_2)\sin(\mu d)\right]i\frac{1}{Y}\sin(\mu y_1)$$

464 $$+\left[\cos(\mu x_2 + \mu d) + iKY\sin(\mu x_2)\cos(\mu d)\right]\left[\cos(\mu y_1) + i\frac{I}{Y}\sin(\mu y_1)\right].$$

465 By applying the initial and boundary conditions of the PRV system shown in Fig. 1 (i.e.,
466 $h^{Up} = q^{Dn} = 0$ in the frequency domain), the TFR results obtained for the above two cases are
467 given by Eq. (15) and Eq. (16) respectively in the text.

468

469 **References**

470 Adewumi M.A., Eltohami E.S., and Solaja A. (2003). Possible detection of multiple blockages
471 using transients. *Journal of Energy Resources Technology* 125, 154-159.

472 AWWA (American Water Works Association). (2012). *Buried No Longer: Confronting America's*
473 *Water Infrastructure Challenge*. AWWA Report, pp. 37.

474 Brunone B. (1999). Transient test-based technique for leak detection in outfall pipes. *Journal of*
475 *Water Resources Planning and Management – ASCE*, 125(5), 302-306.

476 Chaudhry M.H. (2014). *Applied Hydraulic Transients (3rd Ed)*. Springer, New York.

477 Che T.C., Duan H.F., Lee P.J., Pan B., and Ghidaoui M.S. (2018). Transient frequency responses
478 for pressurized containing blockages with linear varying diameters. *Journal of Hydraulic*
479 *Engineering – ASCE*, 144(8), 04018054.

480 Covas D., Ramos H., and De Almeida A. (2005). Standing wave difference method for leak
481 detection in pipeline systems. *Journal of Hydraulic Engineering – ASCE*, 131(12), 1106–
482 1116.

483 Datta S., and Sarkar S. (2016). A review on different pipeline fault detection methods. *Journal of*
484 *Loss Prevention in the Process Industries*, 41(2016), 97-106.

485 Duan H.F., Lee P.J., Ghidaoui M.S., and Tung Y.K. (2010). Essential system response
486 information for transient-based leak detection methods. *Journal of Hydraulic Research –*
487 *IAHR*, 2010. 48(5), 650-657.

488 Duan H.F., Lee P.J., Ghidaoui M.S., and Tung Y.K. (2011). Leak detection in complex series
489 pipes by system frequency response method. *Journal of Hydraulic Research – IAHR,* 49(2),
490 213-221.

491 Duan H.F., Lee P.J., Ghidaoui M.S., and Tung Y.K. (2012a). Extended blockage detection in

492 pipelines by using system frequency response analysis. *Journal of Water Resources*
493 *Planning and Management – ASCE*, 138(1), 55-62.
494 Duan H.F., Ghidaoui M.S., Lee P.J., and Tung Y.K. (2012b). Relevance of unsteady friction to
495 pipe size and length in pipe fluid transients. *Journal of Hydraulic Engineering – ASCE*,
496 138(2), 154-166.
497 Duan H.F., Lee P.J., Ghidaoui, M.S., Tuck J. (2014). Transient wave-blockage interaction and
498 extended blockage detection in pipelines. *Journal of Fluids and Structures,* 46(1), 2-16.
499 Duan H.F. (2015). Uncertainty analysis of transient flow modeling and transient-based leak
500 detection in elastic water pipelines. *Water Resources Management*, 29(14): 5413-5427.
501 Duan H.F. (2016). Sensitivity analysis of transient based frequency domain method for extended
502 blockage detection in water pipeline systems. *Journal of Water Resources Planning and*
503 *Management – ASCE*, 142(4), 04015073.
504 Duan H.F., and Lee P.J. (2016). Transient-based frequency domain method for dead-end side
505 branch detection in reservoir-pipeline-valve systems. *Journal of Hydraulic Engineering –*
506 *ASCE*, 142(2), 04015042.
507 Duan H.F., Lee P.J., Che T.C., Ghidaoui M.S., Karney B.W., and Kolyshkin A.A. (2017). The
508 influence of non-uniform blockages on transient wave behavior and blockage detection in
509 pressurized water pipelines. *Journal of Hydro-environment Research*, 17, 1-7.
510 Duan H.F. (2017). Transient frequency response based leak detection in water supply pipeline
511 systems with branched and looped junctions. *Journal of Hydroinformatics – IWA*, 19(1), 17-
512 30.
513 Duan H.F., Che T.C., Lee P.J., and Ghidaoui M.S. (2018). Influence of nonlinear turbulent
514 friction on the system frequency response in transient pipe flow modelling and

515 analysis. *Journal of Hydraulic Research – IAHR*, 56(4), 451-463,
516 Ghazali M.F., Beck S.B.M., Shucksmith J.D., Boxall J.B., and Staszewski W.J. (2012).
517 Comparative study of instantaneous frequency based methods for leak detection in pipeline
518 networks. *Mechanical Systems and Signal Processing*, 29, 187–200.
519 Gong J., Lambert M.F., Simpson A.R., and Zecchin A.C. (2013). Single-event leak detection in
520 pipes using first three resonant responses. *Journal of Hydraulic Engineering – ASCE*, 139(6),
521 645–655.
522 Gong J., Lambert M.F., Simpson A.R., and Zecchin A.C. (2014). Detection of localized
523 deterioration distributed along single pipelines by reconstructive MOC analysis. *Journal of*
524 *Hydraulic Engineering – ASCE*, 140(2), 190-198.
525 Gong J., Lambert, M.F., Zecchin A.C., and Simpson A.R. (2016). Experimental verification of
526 pipeline frequency response extraction and leak detection using the inverse repeat
527 signal. *Journal of Hydraulic Research – IAHR*, 54(2), 210-219.
528 Gong J., Lambert M.F., Nguyen S., Zecchin A.C., and Simpson, A.R. (2018). Detecting thinner-
529 walled pipe sections using a spark transient pressure wave generator. *Journal of Hydraulic*
530 *Engineering – ASCE*, 144(2), 06017027(1-8).
531 Gupta A., and Kulat K.D. (2018). A selective literature review on leak management techniques
532 for water distribution system. *Water Resources Management*, 32(10), 3247-3269.
533 HK-WSD (Water Supplies Department of the Hong Kong Government). (2019). Gateway
534 Website at: *http://www.wsd.gov.hk/en/home/index.html*.
535 Kapelan Z.S., Savic D.A., and Walters G.A. (2003). A hybrid inverse transient model for leakage
536 detection and roughness calibration in pipe networks. *Journal of Hydraulic Research –*
537 *IAHR*, 41(5), 481–492.

538 Kim, S.H. (2005). Extensive development of leak detection algorithm by impulse response
539 method. *Journal of Hydraulic Engineering – ASCE*, 131(3), 201-208.
540 Kim, S.H. (2017). Multiple leakage function for a simple pipeline system. *Water Resources*
541 *Management*, 31(9), 2659-2673.
542 Louati M., Meniconi M., Ghidaoui M.S., and Brunone B. (2017). Experimental study of the
543 eigenfrequency shift mechanism in blocked pipe system. *Journal of Hydraulic Engineering*
544 *– ASCE*, 143 (10), 04017044.
545 Lee, P.J., Duan, H.F., Ghidaoui, M.S., and Karney, B.W. (2013). "Frequency domain analysis of
546 pipe fluid transient behaviors. *Journal of Hydraulic Research – IAHR*, 51(6), 609-622.
547 Lee P.J., Duan H.F., Tuck J., and Ghidaoui M.S. (2015). Numerical and experimental study on
548 the effect of signal bandwidth on pipe assessment using fluid transients. *Journal of*
549 *Hydraulic Engineering – ASCE*, 141(2), 04014074.
550 Lee P.J., Lambert M.F., Simpson A.R., Vítkovský J.P., and Liggett J. (2006). Experimental
551 verification of the frequency response method for pipeline leak detection. *Journal of*
552 *Hydraulic Research – IAHR*, 44(5), 693-707.
553 Lee P.J., Vitkovsky J.P., Lambert M.F., Simpson A.R., and Liggett J.A. (2008). Discrete blockage
554 detection in pipelines using the frequency response diagram: numerical study. *Journal of*
555 *Hydraulic Engineering – ASCE*, 134(5), 658-663.
556 Liggett J.A., and Chen L.C. (1994). Inverse transient analysis in pipe networks. *Journal of*
557 *Hydraulic Engineering – ASCE*, 120(8), 934-954.
558 Liou C.P. (1998). Pipeline leak detection by impulse response extraction. *Journal of Fluids*
559 *Engineering – ASME*, 120(4), 833–838.
560 Massari C., Yeh T.C.J., Ferrante M., Brunone B., and Meniconi S. (2014). Detection and sizing

561 of extended partial blockages in pipelines by means of a stochastic successive linear
562 estimator. *Journal of Hydroinformatics*, 16(2),248-258.
563 Meniconi S., Brunone B., Ferrante M., Capponi C., Carrettini C.A., Chiesa C., Segalini D., and
564 Lanfranchi E.A. (2015). Anomaly pre-localization in distribution–transmission mains by
565 pump trip: preliminary field tests in the Milan pipe system. *Journal of Hydroinformatics –*
566 *IWA*, 17(3), 377-388.
567 Meniconi S., Duan H.F., Lee P., Brunone B., Ghidaoui M., and Ferrante, M. (2013).
568 Experimental investigation of coupled frequency- & time-domain transient-based techniques
569 for blockage detection in pipelines. *Journal of Hydraulic Engineering – ASCE*, 139(10),
570 1033-1040.
571 Meniconi S., Brunone B., Ferrante M., and Capponi C. (2016). Mechanism of interaction of
572 pressure waves at a discrete partial blockage. *Journal of Fluids and Structures*, 62, 33-45.
573 Puust R., Kapelan Z., Savic D.A., and Koppel T. (2010). A review of methods for leakage
574 management in pipe networks. *Urban Water Journal*, 7(1), 25-45.
575 Sattar A.M., Chaudhry M.H., and Kassem A.A. (2008). Partial blockage detection in pipelines by
576 frequency response method. *Journal of Hydraulic Engineering – ASCE*, 134(1), 76-89.
577 Stephens M. (2008). Transient response analysis for fault detection and pipeline wall condition
578 assessment in field water transmission and distribution pipelines. *PhD Dissertation*,
579 University of Adelaide, Australia.
580 Stephens M., Lambert M., and Simpson A. (2012). Determining the internal wall condition of a
581 water pipeline in the field using an inverse transient. *Journal of Hydraulic Engineering –*
582 *ASCE*, 139 (3), 310-324.
583 Sun J.L, Wang R.H., and Duan H.F. (2016). Multi-fault detection in water pipes using transient

584 time-frequency analysis. *Journal of Hydroinformatics – IWA*, 18(6), 975-989.
585 Vardy, A.E., and Brown, J.M.B. (2003). Transient turbulent friction in smooth pipe flows.
586 *Journal of Sound and Vibration*, 259(5), 1011-1036.
587 Vitkovsky J.P., Simpson A.R., and Lambert M.F. (2000). Leak detection and calibration using
588 transients and genetic algorithms. *Journal of Water Resources Planning and Management –*
589 *ASCE*, 126(4), 262–265.
590 Wylie E.B., Streeter V.L., and Suo L.S. (1993). *Fluid Transients in Systems*. Prentice-Hall, New
591 Jersey.
592 Zielke, W. (1968). Frequency-dependent friction in transient pipe flow. *Journal of Basic*
593 *Engineering – ASME*, 90(1), 109-115.

Table 1 Experimental application results

Test no.	Leakage				Partial blockage			
	x_1/L	ε_{x1} (%)	K (10^{-6}m^2/s)	ε_K (%)	y_1/L	ε_{y1} (%)	I (10^4s/m^2)	ε_I (%)
E1	0.204	3.43	−6.25	-9.44	0.089	1.12	−2.20	5.45
E2	0.561	1.43	−8.39	-5.60	0.089	4.49	−2.20	10.45

Table 2 Settings of parameters for numerical applications ("*NA*" = not applicable)

Test no.	**Intact pipeline**			**Leakage**		**Partial blockage**		Re_0
	L (m)	D (m)	A (m/s)	x_1/L	K (10^{-5}m^2/s)	y_1/L	I (10^4s/m^2)	
N1	1000	0.2	1200	0.45	−0.079	*NA*	0	1.0×10^4
N2	1000	0.2	1200	*NA*	0	0.60	−12.73	1.0×10^4
N3	1000	0.2	1200	0.20	−0.079	0.70	−12.73	1.0×10^4
N4	1500	0.4	1000	0.35	−0.16	0.45	−3.18	2.0×10^4
N5	1500	0.5	900	0.85	−2.36	0.30	−0.64	8.0×10^4
N6	3000	0.3	1400	0.30	−2.36	0.65	−0.85	1.0×10^5
N7	400	0.5	1100	0.75	−19.64	0.12	−0.23	4.0×10^5
N8	1200	0.8	800	0.60	−117.81	0.25	−0.025	1.0×10^6

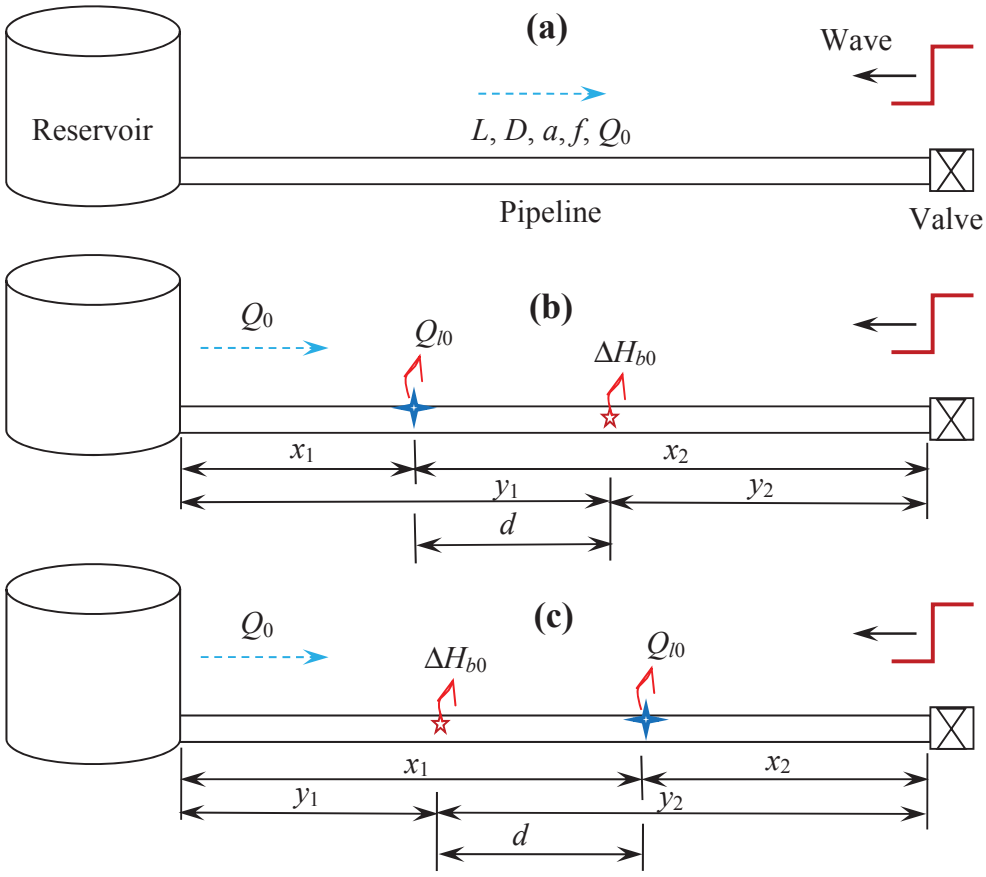

Fig. 1 The RPV systems adopted for investigation: (a) intact pipeline; (b) pipeline with upstream leakage and downstream partial blockage; (c) pipeline with upstream partial blockage and downstream leakage (Q_{l0} for leakage orifice discharge; H_{b0} for blockage minor loss)

Figure 2 Click here to access/download;Figure;Fig2.pdf

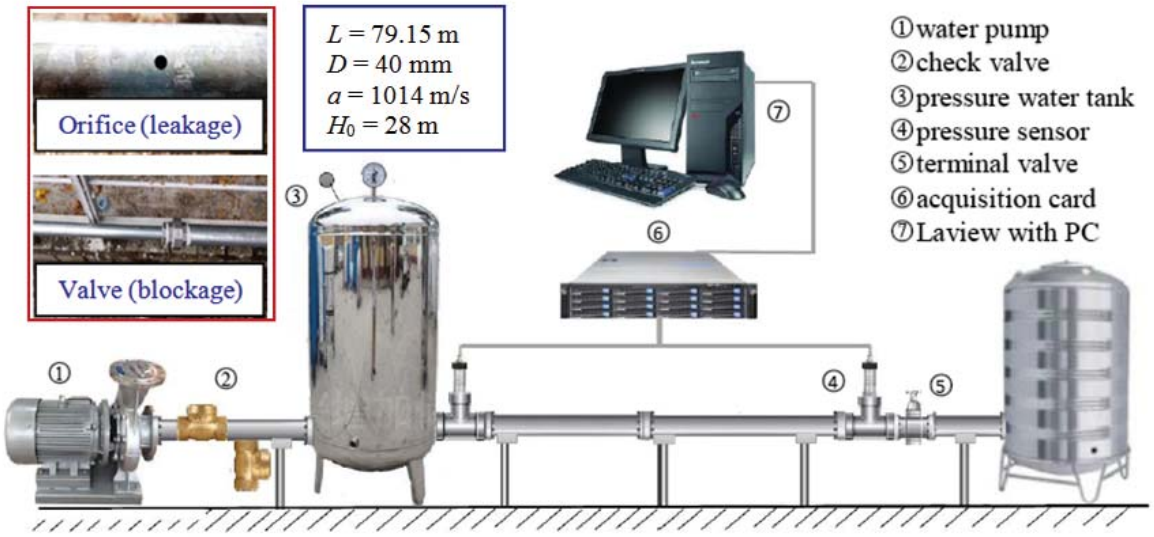

Fig. 2 Sketch of laboratory experimental system and test facilities

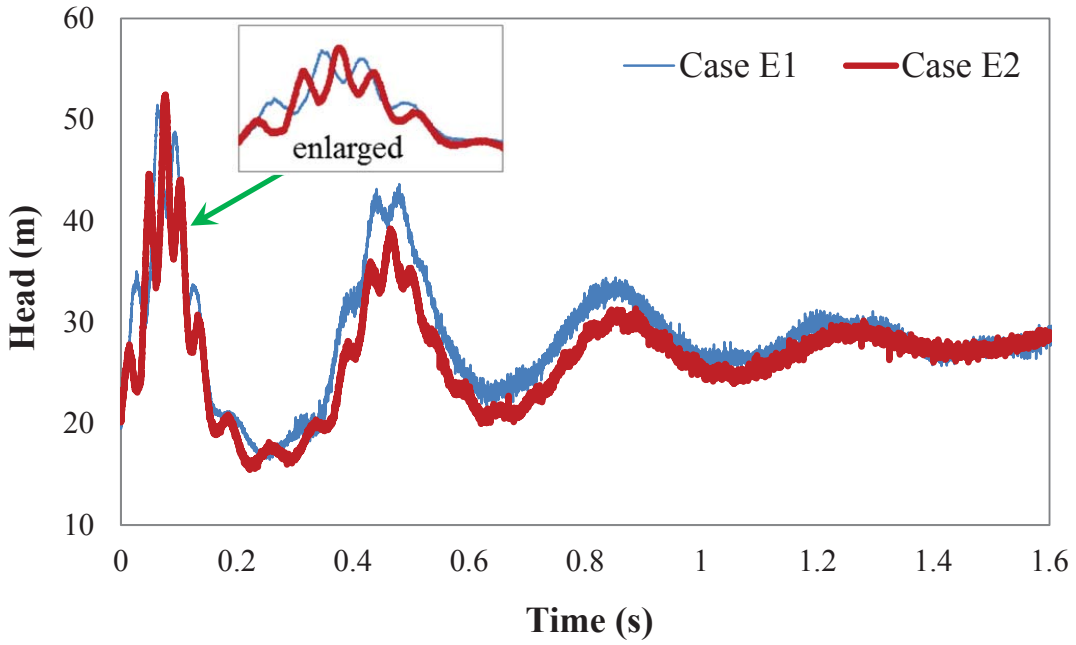

Fig. 3 Measured transient pressure signals for the two experimental test cases

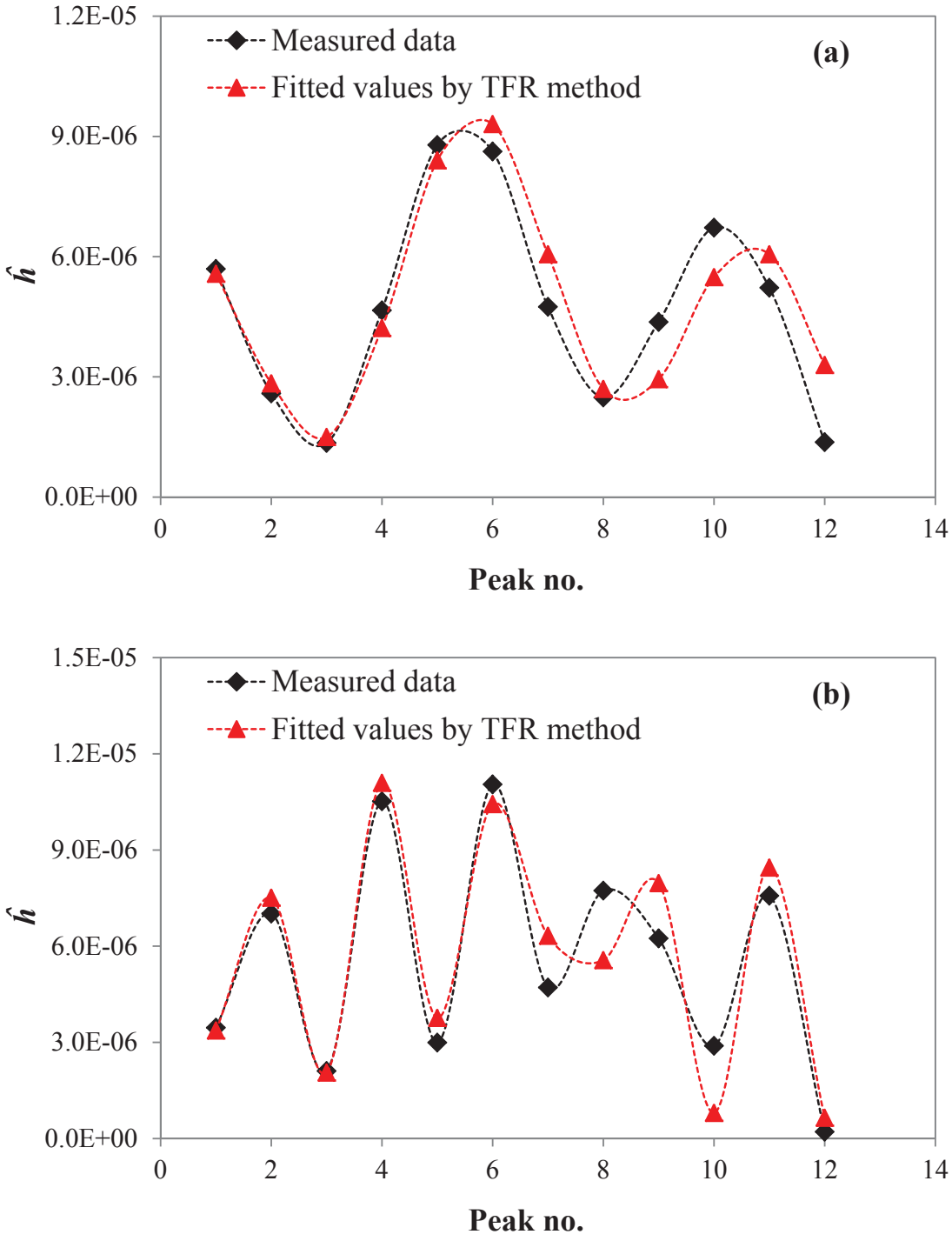

Fig. 4 Results of TFR-based patterns for experimental test cases E1 and E2

Figure 5

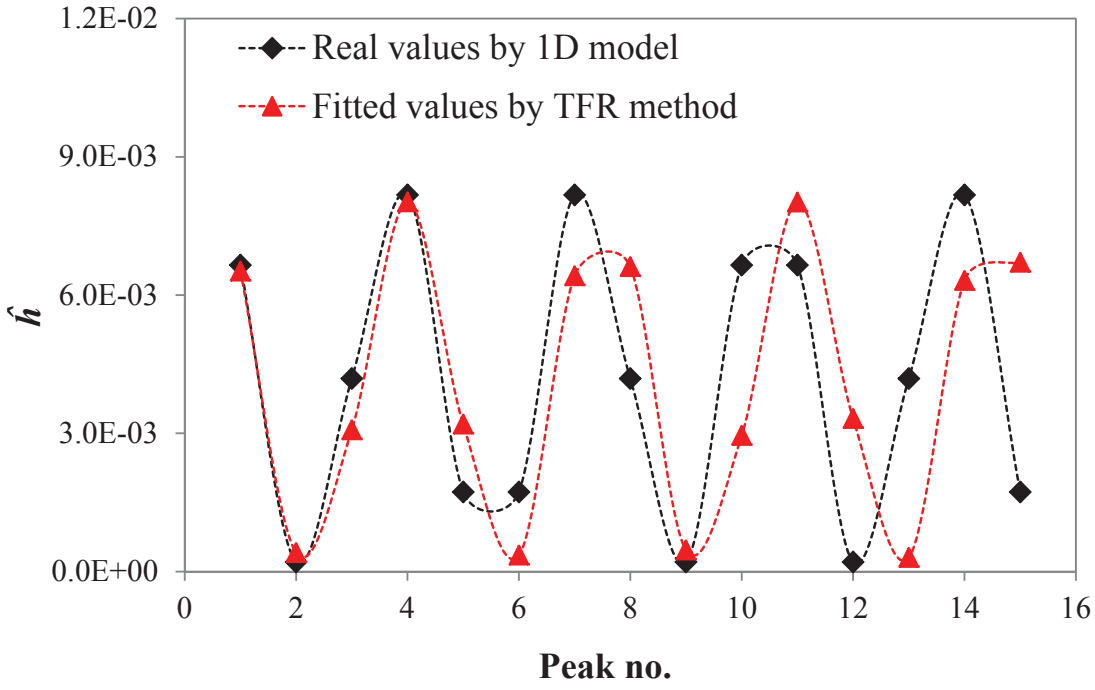

Fig. 5 Results of TFR patterns for case N3 by numerical modelling ("real values") and analytical Eq. (18) fitting ("predicted values")

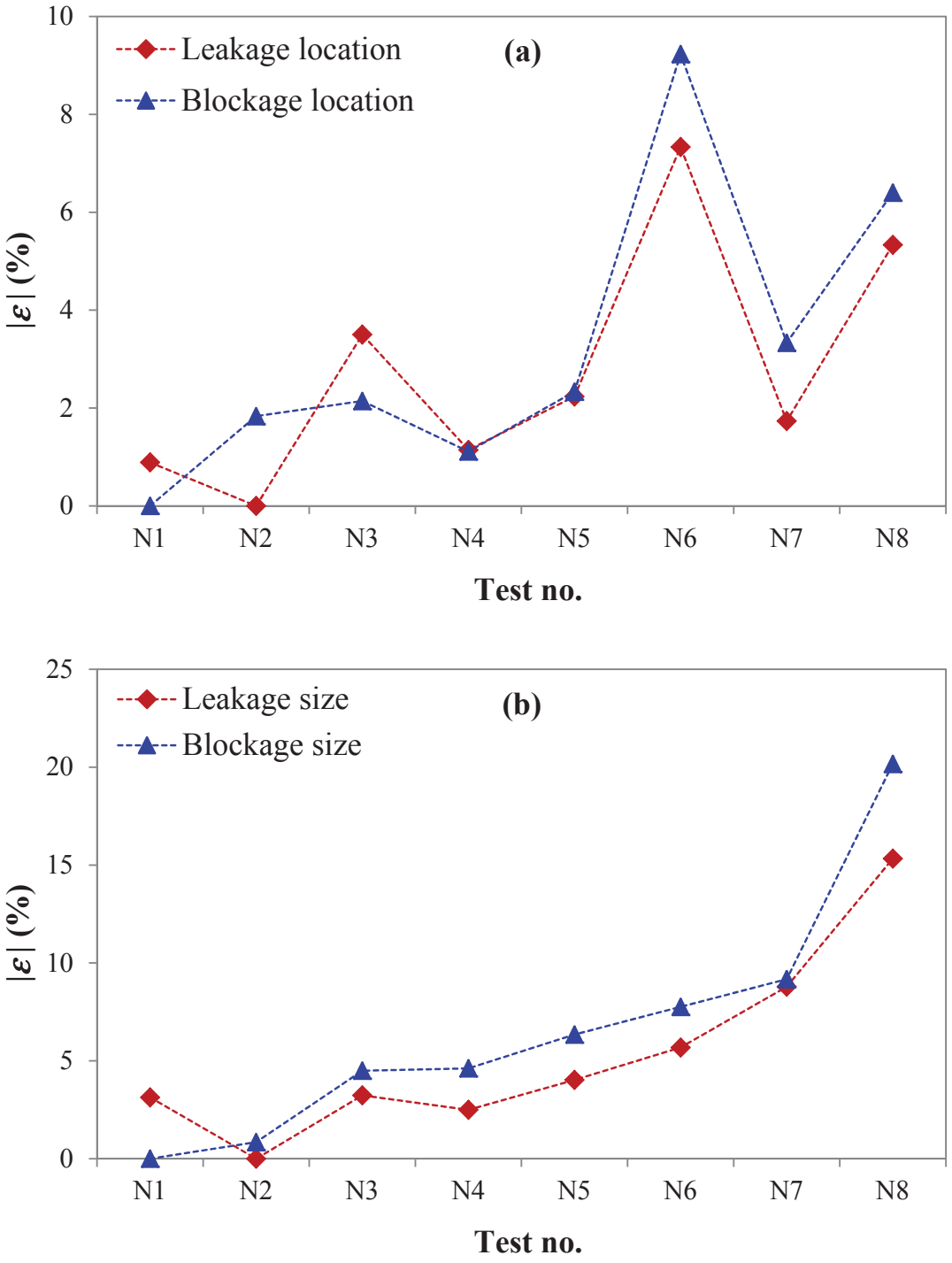

Fig. 6 Relative errors of TFR-based detection results of two defects: (a) location; (b) size

Figure 7

Click here to access/download;Figure;Fig7.pdf

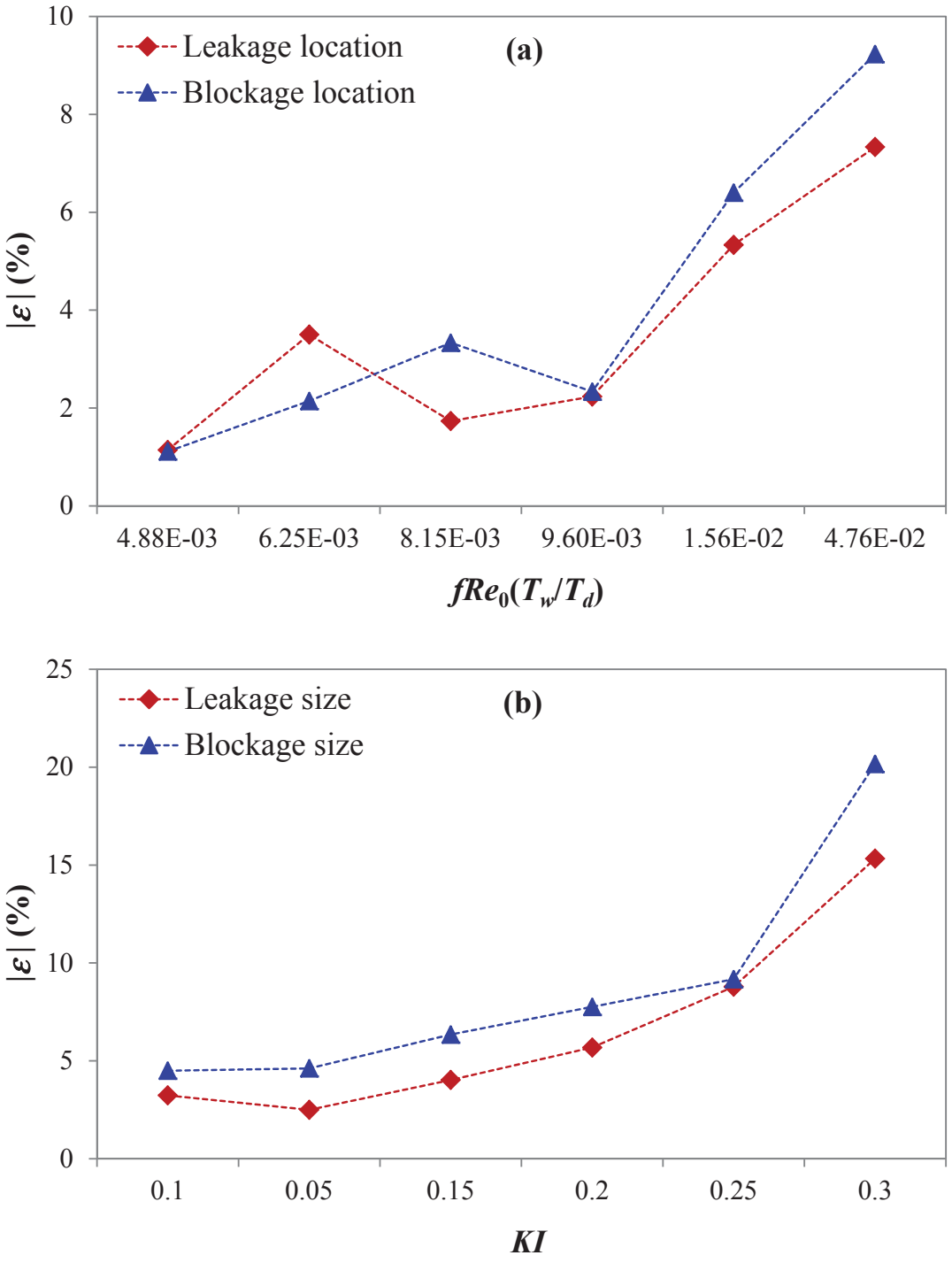

Fig. 7 Accuracy variation of detection results with different system and flow parameters: (a) defect location; (b) defect size

List of Figure Captions

Fig. 1 The RPV systems adopted for investigation: (a) intact pipeline; (b) pipeline with upstream leakage and downstream partial blockage; (c) pipeline with upstream partial blockage and downstream leakage (Q_{l0} for leakage orifice discharge; H_{b0} for blockage minor loss)

Fig. 2 Sketch of laboratory experimental system and test facilities

Fig. 3 Measured transient pressure signals for the two experimental test cases

Fig. 4 Results of TFR patterns for experimental test cases E1 and E2

Fig. 5 Results of TFR patterns for case N3 by numerical modelling ("real values") and analytical Eq. (18) fitting ("predicted values")

Fig. 6 Relative errors of TFR-based detection results of two defects: (a) location; (b) size

Fig. 7 Accuracy variation of detection results with different system and flow parameters: (a) defect location; (b) defect size